



# Heat band, rain band and heat low migration: process-based evaluation of some CMIP6 GCMs over West Africa

Thompson Annor<sup>1</sup> · Apphia Tetteh Ackon<sup>1</sup> · Rachel James<sup>2,3</sup> · Ellen Dyer<sup>3</sup> · Thomas Webb<sup>3,4</sup> · Wilfried Mba Pokam<sup>5</sup> · Giresse Kuete Gouandjo<sup>6</sup> · Richard Washington<sup>3</sup> · Babatunde J. Abiodun<sup>7</sup>

Received: 1 August 2022 / Accepted: 13 August 2023 / Published online: 7 September 2023  
© The Author(s) 2023

## Abstract

Climate model evaluation presents a crucial pathway into the investigation of the simulation of future climate. It presents the only lens through which the future states of the climate of the planet can be explored. In this study, reference datasets including reanalysis products have been used to demonstrate the climatological annual migration of the West African Monsoon System (WAMS) in three components, namely, the West African Heat Low (WAHL), the West African Heat Band (WAHB) and the West African Rain Band (WARB). We have used 8 Global Climate Models (GCMs) from the Coupled Model Intercomparison Project Phase 6 (CMIP6) to assess how the models represent the climatological annual migration of these three features over the same domain for the same period. The results show close linkages between the WAHL, WAHB and the WARB as signature components of the WAMS in their climatological annual dynamics. All three features migrate from the south (with the minimum intensities) in January to the north (with the maximum intensities) in August over the region. The GCMs represent the climatological annual dynamics of all three features to some extent. However, in most of the models analysed the WAHL is too weak, and the WAHB and WARB are located too far south. Insights from this study can be beneficial for investigations of the future state of the WAMS. Also, development of models for the region should target the improved simulation of these features, specifically the intensity of the WAHL, and the locations of the WAHB and WARB.

**Keywords** Process-based evaluation · CMIP6 · West Africa · Heat low · Rain band · Climatology · Climate models

## 1 Introduction

The West African Monsoon System (WAMS) is a major feature of the large-scale circulation. Hundreds of millions of people depend on rainfall from this system for their livelihoods. Seasonal modulation of the WAMS leads to two contrasting states. Centered on January, north-east trade winds prevail over the entire region of West Africa and are associated with the major dry season where atmospheric conditions are stable, nights relatively cool and the concentration of aerosols in the atmosphere high. Conditions across the region in this season are largely homogenous (Biasutti 2019; Annor et al. 2018; Agyekum et al. 2018; Okafor et al. 2019). By July, prevailing south-westerly trade winds bring moisture from the ocean to the continent (Gu and Adler 2004). During this season the region receives its rains mainly through mesoscale convective systems (Gu and Adler 2004; Jung and Kunstmann 2007). As a result, precipitation and other atmospheric conditions are heterogeneous

✉ Rachel James  
rachel.james@bristol.ac.uk

<sup>1</sup> Department of Meteorology and Climate Science, Kwame Nkrumah University of Science and Technology (KNUST), Kumasi, Ghana  
<sup>2</sup> School of Geographical Sciences, University of Bristol, Bristol, UK  
<sup>3</sup> School of Geography and the Environment, University of Oxford, Oxford, UK  
<sup>4</sup> Department of Chemistry, University of York, York, UK  
<sup>5</sup> Department of Physics, Higher Teacher Training College, University of Yaounde 1, Yaounde, Cameroon  
<sup>6</sup> Laboratory for Environmental Modelling and Atmospheric (LEMAP), University of Yaounde 1, Yaounde, Cameroon  
<sup>7</sup> Climate Systems Analysis Group, Department of Environmental and Geographical Science, University of Cape Town, Cape Town, South Africa

over the region (Annor et al. 2018, 2022; Agyekum et al. 2018; Okafor et al. 2019), although climatologically isohyets align neatly along lines of latitude to reach a minimum at the southern edge of the Sahara. Deep convection, often referred to and co-located with the Intertropical Convergence Zone (ITCZ), occurs south of the location of the convergence of the two trade winds which itself is known as the Intertropical Discontinuity (ITD). Biasutti (2019) attributed the movement of the ITCZ to the transport of moisture into the deep convective region via its lower branch and the transport of energy away from the ITCZ in its upper branch, where the mean position of the ITCZ results in a net energy transfer from the northern hemisphere to the southern hemisphere. The result of this is the cyclical movement of bands of moisture (rain belt) and heat over the West African region (Dixon et al. 2017; Biasutti 2019).

While the WAMS comprises an array of atmospheric features across space and time-scales, there are two key components which are integral to the WAMS and are directly connected to the dynamics that drive the system. The first is the well-known West African Heat Low (WAHL). The second is the anomalous near surface temperature and here we introduce for the first time (to best of our knowledge) an index to characterize this, namely the West African Heat Band (WAHB). The WAHL is an area of extremely high surface temperatures formed by intense solar radiation that coincides with low surface pressures over continental Africa (Lavaysse et al. 2009, 2016; Dixon et al. 2017). The WAHL usually takes the form of a closed low pressure system and, typical of a classic heat-low structure, is identifiable in lower tropospheric thickness anomalies. In July, the heat low is in the core of the Sahara over southern Algeria and northern Mali (Engelstaedter et al., 2015) whereas in January, the feature occurs less frequently and is found far to the south beyond the northern extent of the Congo Basin (Lavaysse et al. 2009, 2016). The vertical extent of the WAHL is bounded within the 700 and 925 hPa levels in the atmosphere (Lavaysse et al. 2009, 2016). According to Thorncroft and Blackburn (1999), the heat low has a strong linkage with the African Easterly Jet (AEJ) at the upper level of the WAHL (700 hPa) in the month of July. They reported that the WAHL plays a crucial role in maintaining the AEJ and its associated meridional gradients in potential vorticity at the 700 hPa level. The West African Heat Band, unlike the classic heat low, is a broad zone of high near-surface temperatures across West and North Africa. It is seen as a broad zone, within which the near-surface temperature exceeds the near-surface temperature of all other areas over the West African region. Like the WAHL, this feature occurs less frequently in the months centered on January and is also located far to the south compared with July. Together, these features set up and maintain the energy gradient required

to drive the WAMS. As indicated above, the WAMS vital output is rainfall, and again for the first time (to the best of our knowledge) we present a third component of the WAMS called the West African Rain Band (WARB). The WARB is an index that characterizes areas as with anomalous rainfall (like the WAHB, these are areas where precipitation within the zone exceeds the precipitation of all other areas over the West African region). These are key, large-scale features which are necessary for global climate models to simulate in order to replicate the WAMS adequately.

The African continent in recent times has received a boost in the analysis of numerical weather prediction and climate models for various weather/climate related investigations (e.g., Mariotti et al. 2011; Drobinski et al. 2007) and the West African region is no exception (e.g., Vigaud et al. 2011; Vellinga et al. 2016; Dixon et al. 2017; Akinsanola et al. 2017; Annor et al. 2018; Annor et al. 2022). This is a welcome development in filling the knowledge gap in the area of climate modeling for the continent. For instance, Klein et al. (2015) simulated the variability in the West African monsoon pattern due to different parameterization schemes of a regional climate model. They found differences between model versions in the WAMS, and attributed this to differences in the intensities of the moist Hadley-type meridional circulation which links the monsoon winds to the Tropical Easterly Jet. Also, Dixon et al. (2017) reported that, climate models with northward Sahara Heat Low biases have enhanced short wave absorption and increased low-level specific humidity due to the Saharan water vapor-temperature feedback. A recent further step in this effort is the LaunchPAD (Priority on African Diagnostics) project which evolved through the Future Climate for Africa (FCFA) ([www.futureclimateafrica.org](http://www.futureclimateafrica.org)) programme. The purpose of this paper, which is part of the LaunchPAD project, is therefore to investigate the structure and dynamics of the WAHL, WAHB and the rainfall response by the WAMS (i.e., the WARB) in coupled climate models. If climate models fail to replicate key large-scale drivers and response of the WAMS, such as the WAHL and WAHB, and WARB, it should not be reasonably expected that the response of these models to future greenhouse gas emissions can be trusted. The investigation in this paper could therefore be construed as an inspection of the necessary first-order features required of a climate model over West Africa. Here we focus on the most recently available ensemble of coupled climate model experiments, namely CMIP6. The data and the method of analysis applied in this study are presented in Sect. 2. Section 3 contains the results and discussion. We provide our summary and conclusions in Sect. 4.

## 2 Data and methods

### 2.1 Data

#### 2.1.1 Reference data

The quality of reference data in a model evaluation process is crucial and for the West African region; specifically, for precipitation; reference datasets created from dense rain gauge measurements are required due to the high spatial variability of precipitation. Temperature on the other hand tends to be more homogenous over the region. Similarly, geopotential fields do not vary much over short distances in the West African region. Two types of reference datasets (satellite-merged-with-gauge and reanalysis) are applied in this study. We used reanalysis datasets for the evaluation of the WAHL and WAHB. In the case of the WARB, the satellite-merged-with-gauge dataset type is used, because the precipitation fields in the reanalysis datasets used for the WAHL and WAHB are assimilated data which could not represent actual precipitation data as accurately as a measured dataset.

The determination of the WARB requires a monthly total precipitation dataset. In this case we used the Global Precipitation Climatology Project (GPCP version 2.3), with a horizontal resolution of  $2.5^\circ \times 2.5^\circ$  covering both the land surface and the oceans of the globe (Adler et al. 2018).

Like the WARB, monthly mean 2-m air temperature dataset is needed for the determination of the WAHB and two different reanalysis datasets are used here. We applied the European Centre for Medium-Range Weather Forecast reanalysis product ERA5 (Hersbach et al. 2020) at  $0.25^\circ \times 0.25^\circ$  horizontal resolution and the Modern-Era Retrospective analysis for Research and Applications, Version 2 (MERRA2) (Rienecker et al. 2011) from the National Aeronautics and Space Administration (NASA). The MERRA2 has  $0.5^\circ \times 0.625^\circ$  horizontal resolution.

The data requirement for identification of the WAHL is 6-hourly geopotential height. ERA-Interim (ERA-IN)

(Berrisford et al. 2011) at  $0.5^\circ \times 0.5^\circ$  horizontal resolution and ERA5 are used.

#### 2.1.2 Model data

Eight Global Climate Model (GCM) simulations from the Coupled Model Intercomparison Project phase 6 (CMIP6) (Eyring et al. 2016) are used. GCMs outputs in CMIP6 are produced by various institutions across the globe. Due to the high temporal resolution requirement for the determination of the WAHL (i.e., 6-hourly geopotential data on various levels), we were constrained in the selection of the GCMs. Thus, the selection of the historical experiments of the 8 models in this study, since their output temporal resolutions are within the required domain that is needed for the determination of the features/processes in this study. The 8 models used in this study (as a result of the above explained constraint) form a small subset of the entire CMIP6 ensemble, however, they can be used adequately to show how some (not necessary a representative sample of) CMIP6 models simulate these features/processes over the region. Further details of the modelled data applied for the study are given in Table 1.

### 2.2 Method

The simulations of the climatological migration of the WARB, WAHB and WAHL are examined in models, and compared to the reference datasets on monthly and seasonal scales over the study domain with longitudes  $20.0^\circ\text{W}$  to  $30.0^\circ\text{E}$  and latitudes  $0^\circ$  to  $40^\circ\text{N}$  (Fig. 1). The precipitation, temperature and geopotential height outputs from the GCMs for the period 1983–2012 were extracted for the determination of the WARB, WAHB and the WAHL, as follows:

**The West African Heat Low** The WAHL is an area of high surface temperatures that coincide with low surface pressures over continental Africa. We applied the Low-Level Atmospheric Thickness (LLAT) approach which has been

**Table 1** Details of models used in the study, with the institutions that produced them, the spatial resolution and references. (Acronym expansions are available online at <http://www.ametsoc.org/PubsAcronymList>.)

Model	Institution	Horizontal Resolution (lon. X lat.)	Vertical Resolution	Reference
CNRM-CM6-1	CMCC	$362 \times 294$	75	Voltaire et al. (2018)
GISS-E2-1G	NASA GISS	$144 \times 90$	40	NASA/GISS (2018)
IPSL-CM6A-LR	IPSL	$144 \times 143$	79	Boucher et al. (2018)
MPI-ESM1-2-HR	MPI	$384 \times 192$	95	Jungclaus et al. (2019)
MPI-ESM1-2-LR	MPI	$192 \times 96$	47	Wieners et al. (2019)
MPI-ESM1-2-HAM	MPI	$192 \times 96$	47	Neubauer et al. (2019)
MRI-ESM2-0	MRI	$320 \times 160$	80	Yukimoto et al. (2019)
NorESM2-LM	NCC	$144 \times 96$	32	Seland et al. (2019)

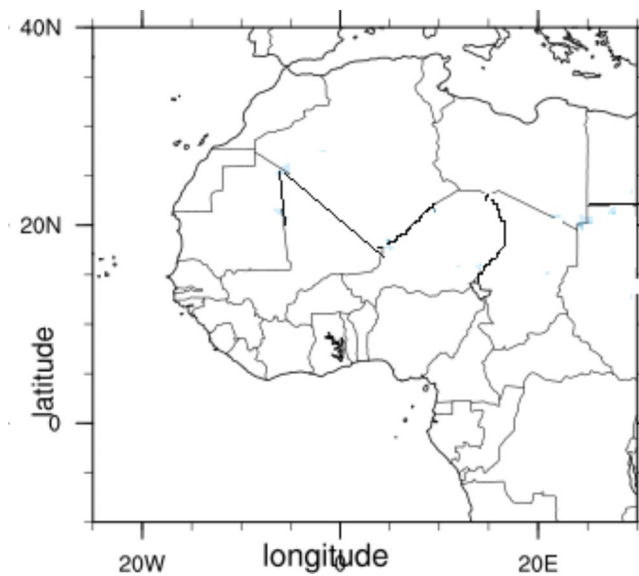


**Fig. 1** The study domain over West Africa

widely used for the detection of the WAHL (e.g. Lavaysse et al. 2009; Lavaysse et al. 2010a, b; Dixon et al. 2017). The LLAT is determined as the geopotential thickness between 700 hPa and 925 hPa using the daily 0600 UTC geopotential heights. According to Lavaysse et al. (2009) the temperature minimum and the pressure maximum are reached in the heat low region shortly before sunrise hence, the used of the 0600 UTC geopotential heights. We then calculated the cumulative probability distribution function of the LLATs on all grids in the study domain (Fig. 1) and finally, defined the WAHL as area with the highest 10% values of LLAT (Lavaysse et al. 2009).

**The West African Heat Band** The WAHB is determined as an area over the West African region with climatological monthly mean 2 m temperature (MMT) above a certain threshold. We computed the cumulative probability distribution function of the MMTs (similar to that of the LLAT) on all grid boxes within the study area (Fig. 1). The WAHB is then defined as the area where the MMT is above 50% of the MMT cumulative probability distribution function (i.e., the highest 50% values of MMT). For example, to determine the climatological WAHB for January, the MMT for January of each year is calculated. So, for the 30-year period used in this case, there are 30 MMTs for January. We then computed the cumulative probability distribution function of MMT on all grid boxes within the domain (Fig. 1) to get the cumulative probability distribution function for the month of January. Then, the WAHB for January is determined as grid boxes within the domain that have MMT with 50% exceedance of the January cumulative probability distribution function for a particular year. This is done for every January in the 30-year period and a mean WAHB is

calculated for the 30-year period for the month January. The process is repeated for rest of the 11 months.

**West African Rain Band** The WARB is an area over West Africa where monthly total precipitation exceeds a threshold. We computed the Monthly Total Precipitation (MTP) for individual months in the study period. Then the cumulative probability distribution function of the MTPs on all grids in the study domain (Fig. 1) is computed. Finally, the WARB is defined as the area with MTP exceeding 50% of the MTP cumulative probability distribution function (i.e., the highest 50% values of MTP). For example, to determine the climatological WARB for January, the MTP of each year is calculated. Similar to the WAHL there are 30 MTPs for January. We then computed the cumulative probability distribution function of MTP on all grid boxes within the domain (Fig. 1) to get the cumulative probability distribution function for the month of January. Then, the WARB for January is determined as grid boxes within the domain that have MTP with 50% exceedance of the January cumulative probability distribution function for a particular year. This is done for every January in the 30-year period and a mean WARB is calculated for the 30-year period. The process is then repeated for rest of the 11 months.

The abilities of the 8 models in representing the location and intensities of the WAHL, WAHB and WARB on monthly and seasonal time scales are assessed using observational/reanalysis datasets as references.

### 3 Results

In this section we present and discuss how the models and reanalyses represent the month-to-month climatological migration of the three features. The seasonal cycle is presented for the zonal heat and rain bands. Maps of the features by the models are used as a general assessment; while metrics applied for the specific assessments are the location, intensity and the shape of the features.

#### 3.1 West African Heat Low (WAHL)

Results for the climatological monthly mean of WAHL for all the datasets including the references are shown in Fig. 2. It is evident from both the ERA-IN and ERA5 results as well as previous studies (e.g., Lavaysse et al. 2009) that the WAHL persists over the study domain every month of the year, which, according to Fig. 2, all the 8 CMIP6 GCMs are also able to generate.

In the reanalysis datasets, the WAHL is located at the south-eastern (the southernmost position) part of the

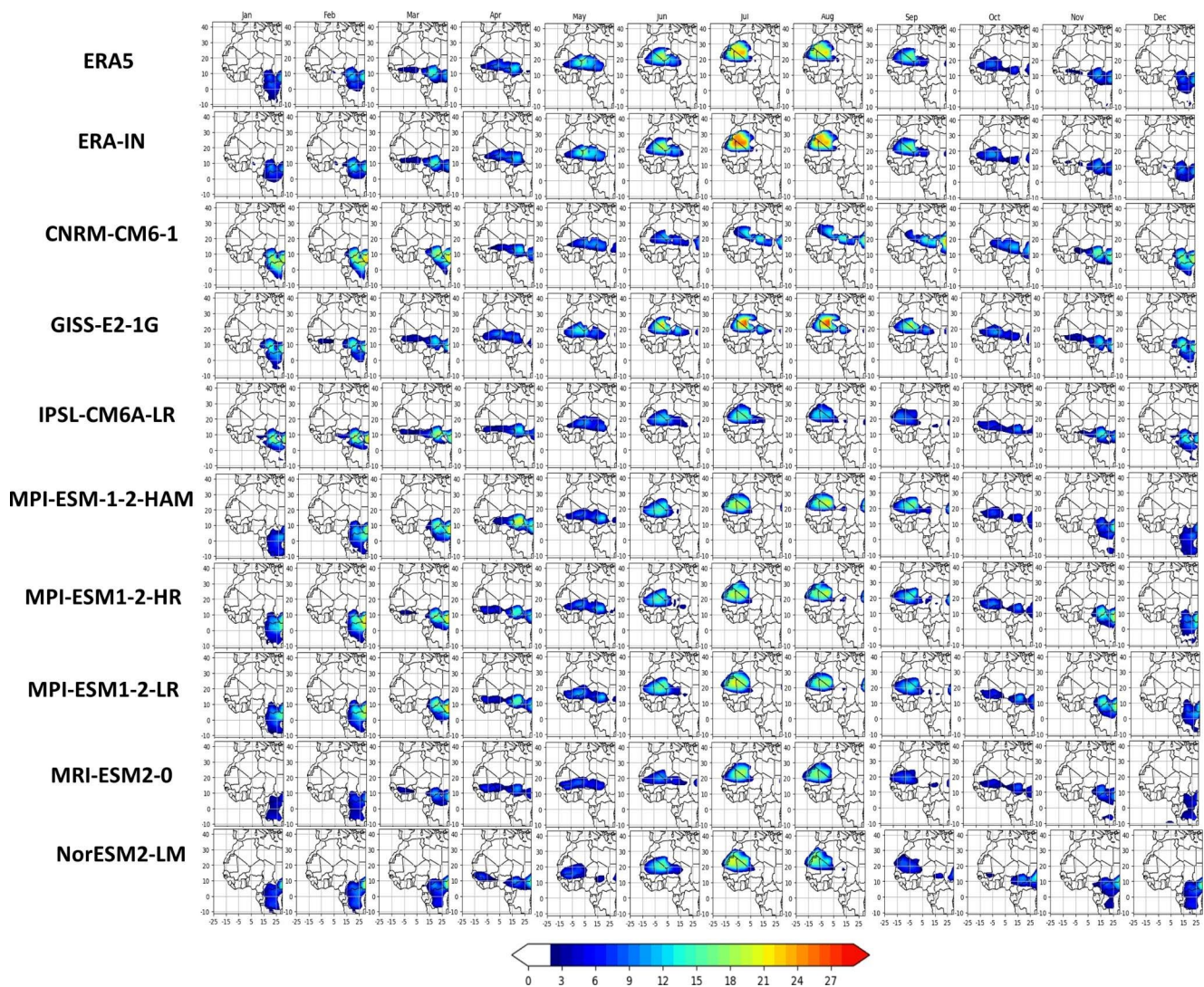


**Fig. 2** Maps of monthly mean occurrence of the WAHL for the 1983–2012 climatological period for the references and the 8 CMIP6 GCMs. These characterize the detection procedure of the heat low in grid

domain (over eastern Central African Republic) in January and thereafter it moves diagonally to the north-western (the northernmost position) part of the region (the Sahara region) in August. It then transverses back to the south-eastern location in December to complete the annual cycle. There are some uncertainties (though not significant) in the location of the WAHL in January in the two reanalysis products. The January WAHL generated in ERA5 covers a wider area (more latitudes) than in ERA-IN. These results (especially the ERA-IN) are in agreement with earlier studies done on the WAHL (e.g., Lavaysse et al. 2009; Lavaysse et al. 2010a; Dixon et al. 2017). The north-south movement of the WAHL has been linked to the migration of the solar radiation (Lavaysse et al. 2009). The results in Fig. 2 indicate that all the GCMs used in this study are generally able to reproduce the climatological monthly location of the

boxes as the top 10% of LLAT values, and the colour bar shows the heat low intensity in m (i.e., anomaly in the geopotential height)

WAHL, however differences exist in the simulations of the location of the WAHL in the models. According to Semazzi and Sun (1997), Drobinski et al. (2007) and Lavaysse et al. (2009) the westward movement from January to August could be attributed to the leeward depression of the Air and Hoggar mountains that generate anomalous geopotentials; and it can be inferred from the results that this effect is generally represented in the models. The degree of difference seen in the reference datasets also exists in the models. While only IPSL-CM6A-LR simulates the southernmost location of the WAHL in January similarly to ERA-IN, all the other 7 models simulate the WAHL's location in January similarly to ERA5. The location of the WAHL in August by the CNRM-CM6-1 model extends further east of the Sahel region, whereas in the case of the MPI models a smaller secondary heat low is located at the eastern part of the Sahel

region. The location of the WAHL in the month of August over the Sahel by the CNRM-CM6-1 model is much influenced by the shape of the simulated WAHL. According to Lavaysse et al. (2009), a heat low is formed at a particular location over the West African region when there exists a low atmospheric pressure closer to the surface which results from lower tropospheric heating and the ensuing lifting of isobaric surfaces and divergence of air upward. The application of the LLAT ensures the elimination of heat low formation due to deep planetary boundary layer mixing as result of afternoon heating and/or extra-tropical forcing (Lavaysse et al. 2009). In August in the CNRM-CM6-1 simulation, this system of lower tropospheric heating and the resulting lifting of isobaric surfaces and divergence of air aloft spreads across almost the entire Sahel region. Whereas in the MPI models' simulations this feature occurs at an additional location in the eastern part of the Sahel.

Following closely to the month-to-month location is the intensity of the WAHL, where it starts increasing in intensity from January, reaching a maximum in August, and thereafter (from September) decreasing to a minimum in December, as shown in the reanalysis datasets in Fig. 2. High intensities of the WAHL in June, July and August (mainly the summer monsoon months (Sylla et al. 2009; Marshall et al. 2014; Biasutti 2019)) have the location in the Sahara region, which is consistent with studies including Lavaysse et al. (2009, 2010a) and Dixon et al. (2017), hence the name Sahara Heat Low (Ramel et al. 2006). The intensity is slightly stronger in ERA-IN than ERA5. Similarly, some variations are seen in the simulation of the intensity of the WAHL by the models. Models such as CNRM-CM6-1, IPSL-CM6A-LR, NorESM2-LM, MPI-ESM1-2-HAM, MPI-ESM1-2-HR and MPI-ESM1-2-LR simulate generally stronger intensities than the reanalyses for the dry season (winter) months (November-March) and weaker for the wet season (summer) months (May to August). The GISS-E2-IG model for instance simulates slightly stronger intensities than ERA-IN for all months, especially the core of the heat low in July and August, while MRI-ESM2-0 simulates weaker intensities than ERA5 for all months.

The WAHL assumes a circular shape in the dry (winter) season months (December to February), and the wet (summer) season months (May to September). Then, its shape/form changes into an elongated structure for the March, April (in spring), October and November (in autumn) months (Fig. 2). Similar shapes have been reported in earlier studies of the heat low over the region (e.g., Lavaysse et al. 2009; Dixon et al. 2017). In general, these two shapes are all present in all the CMIP6 models used for this study. Models such as IPSL-CM6A-LR and GISS-E2-1G have similar shapes as the reanalysis products. The NorESM2-LM and the MPI-models have circular shapes for November to March, thus

prolonging the period of the circular shape for the dry (winter) season. While the MPI models shorten the period for the circular shape for the wet season (summer) months (from June to September), in the case of the NorESM2-LM model, it is similar (May to September) to the reanalysis products. The NorESM2-LM model simulates the shortest period (April and October) for the elongated shape, followed by the 3 MPI models (April, May and October) in comparison with the reference datasets. The MRI-ESM2-0 model simulates the circular shape earlier (November to February) for the dry season than the reanalysis (December to February) and later (July to September) than the reanalysis (May to September) for the summer season. The CNRM-CM6-1 model is quite unique among the models and the reanalysis products in that the circular shape in the wet (summer) months is not present. The circular shape of the WAHL in the winter and summer seasons months has been attributed to the very intense cyclonic circulation that prevails in the vicinity of the WAHL (Lavaysse et al. 2009) and in general, the models are fairly representing this very intense cyclonic circulation except CNRM-CM6-1 in summer. This could mean that the appropriate circulation in the summer season months (which is also crucial for rainfall over the region) is poorly represented in the CNRM-CM6-1 model in particular.

## 3.2 West African Heat Band (WAHB)

### 3.2.1 Spatial structure of the WAHB

The WAHB is an approach to locate the part of the region (with respect to latitude) where higher temperature (the highest 50% values of MMT) is located. It has been reported in several studies (e.g., Dixon et al. 2017; Biasutti 2019) that anomalous heating either in the northern or southern hemisphere is responsible for north-south movement of the ITCZ. We therefore present the results of migration of the WAHB for the 2 reanalysis products and the 8 CMIP6 GCMs in this section.

In January (Fig. 3), the WAHB in both ERA5 and MERRA2 is located in the southern part (south of 18°N) of the domain. It then moves gradually northwards with increasing intensity, especially over the continent in April. While still a lower intensity of the WAHB lingers around the ocean south of 10°N, the northwards progression continues with the increasing intensity from May to August where the northernmost position (north of 15°N) and highest intensity is attained over the Sahel and the Sahara. This northwards migration of the WAHB (which is similar to the northwards migration of the WAHL) from January to August could be linked to the migration of incoming shortwave radiation, as mentioned in Lavaysse et al. (2009). From May to August

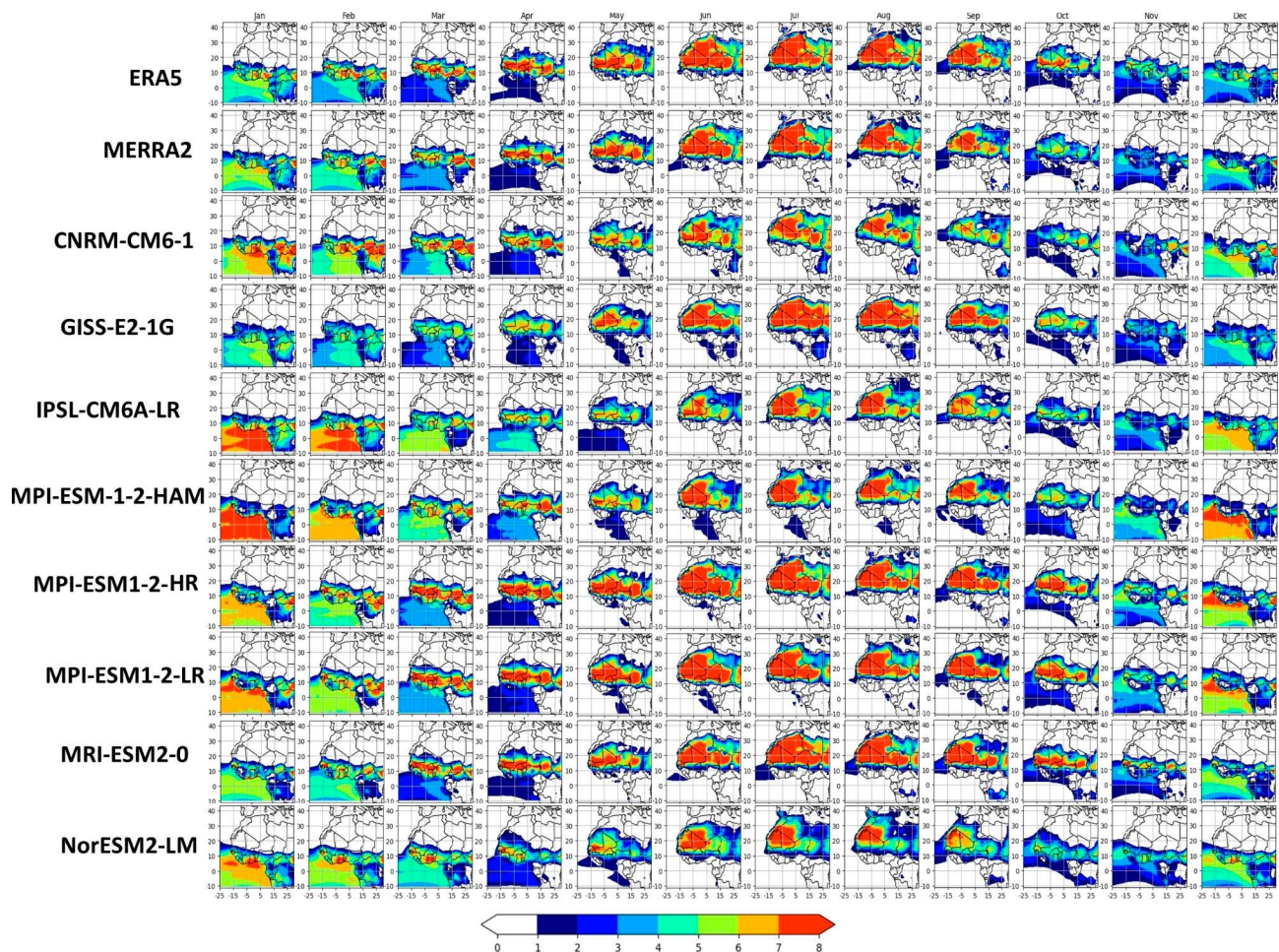


**Fig. 3** Maps of monthly mean WAHB for the 1983–2012 climatological period for the references and the 8 CMIP6 GCMs. The colour bar shows heat band intensity (near surface temperature) in °C

the WAHB is mainly located over the continent and the parts over the ocean vanish. From September, its intensity reduces, retreats southwards and the part over the ocean begins to appear, until December where it reaches its southernmost (south of 18°N) location over both ocean and continent. The results show that the WAHB has higher intensities over the continent than over the ocean. This could be due to the different partitioning of incoming solar radiation over the continent and the ocean. In general, a greater portion of the incoming solar radiation is converted into sensible heat than latent heat over the continent and the reverse is the case over the ocean, where also heat is transferred to deeper depths. It is widely known that surface heating increases the thickness of the Planetary Boundary Layer (PBL), it is then consistent that the migration of the WAHB and the locations of the highest intensity follow closely to that of the WAHL. This is because the LLAT approach used in this study for the determination of the WAHL is highly controlled by the surface heating (Drobinski et al. 2005; Lavaysse et al. 2009; Dixon et al. 2017). The similarity in the annual migration of

both the WAHB and the WAHL clearly confirms the strong linkage between the West African Monsoon (WAM) and both the WAHL (Chauvin et al. 2010; Lavaysse et al. 2010a) and the WAHB.

There are some differences in the simulations of the WAHB in the models especially with respect to the intensity. For the winter (dry) season (DJF) months, models such as CNRM-CM6-1, NorESM2-LM, IPSL-CM6A-LR, MPI-ESM1-2-HR and MPI-ESM1-2-LR (Fig. 3) simulate in general stronger WAHB intensities than the reanalysis products over both ocean and the continent. This result is consistent with studies that have reported the simulation of warm biases over the Gulf of Guinea by models (e.g., McCrary et al. 2014; Zuidema et al. 2016). MPI-ESM1-2-HAM simulates the strongest intensities of the WAHB over the ocean, but slightly weaker intensities over the continent in comparison to the reanalysis datasets. These biases could result in the simulation of enhanced evaporation over the ocean in the model. MRI-ESM2-0 and GISS-ESM-E2-1G

simulate the reanalysis products' WAHB intensities for the winter months quite closely.

In March and April, CNRM-CM6-1, NorESM2-LM, IPSL-CM6A-LR and MPI-ESM1-2-HAM (Fig. 3) reproduce slightly stronger (weaker) intensities of the WAHB over the ocean (continent) in comparison to the reanalysis products. This result in the models' simulations could lead to the simulations of more evaporation over the ocean in the models. While MPI-ESM1-2-HR and MPI-ESM1-2-LR simulate slightly stronger intensities, GISS-ESM-E2-1G on the other hand, simulates slightly weaker intensities over both land and ocean compared to the references. The MRI-ESM2-0 model simulated the WAHB intensities similar to that of the MERRA2.

The West African region receives most of its annual rains in the summer monsoon months of May to September (Hagos and Cook 2007; Dixon et al. 2017) and according to the reference datasets, the strongest intensities of the WAHB occur in larger areas exclusively over the continent. In these months, CNRM-CM6-1, NorESM2-LM, IPSL-CM6A-LR and MPI-ESM1-2-HAM (Fig. 3) generally simulate slightly weaker intensities of the WAHB than the reanalysis datasets. Earlier studies including Thorncroft and Blackburn (1999), Ramel et al. (2006), Hagos and Cook (2007), Hsieh and Cook (2008), Dixon et al. (2017) have reported that the monsoon circulation that brings moisture from the ocean onto the continent is substantially influenced by the maximum meridional temperature gradient that exists over the West African region in these months. The simulation of weaker WAHB intensities for these months in these models may lead to a reduced temperature gradient which could hamper the simulation of moisture flux from the ocean onto the continent. In other models (MRI-ESM2-0, GISS-ESM-E2-1G, MPI-ESM1-2-HR, MPI-ESM1-1-LR) the intensity of the WAHB in May to September is more similar to that of reanalysis products, although, there are some months and some models where the WAHB is slightly stronger in the models than in reanalyses. This may be associated with slightly stronger moisture fluxes.

The WAHB in October and November has patterns similar to that in March and April, though intensities are stronger in the spring months than the autumn months. Models such as CNRM-CM6-1, NorESM2-LM and GISS-ESM-E2-1G (Fig. 3) have WAHB intensities that fall within the values shown by the two reanalysis products. IPSL-CM6A-LR and MPI-ESM1-2-HAM simulate intensities similar to MERRA2. The MRI-ESM2-0, MPI-ESM1-2-HR and MPI-ESM1-2-LR models simulated slightly stronger intensities for October and November in comparison to the references. Like the rest of the months; the simulation of the WAHB (especially in terms of the intensity) for these months are fairly done by the models since the variations from one

model to another are generally within the range of the uncertainties that are seen in the reference datasets. These results suggest that the models are representing the north-south migration of incoming solar radiation quite similarly to the reference datasets.

### 3.2.2 Zonal structure of the WAHB

The climatological monthly mean time - latitude Hovmoeller diagrams of the WAHB for all the datasets are shown in Fig. 4, illustrating the seasonal cycle of the WAHB.

In the winter season (DJF) months, the highest intensities of the heat band (but rather relatively low – less than 6 °C, but greater than 4 °C) are seen mostly between 4°S and 12°N in the reanalysis products. This result is consistent with that of Lavaysse et al. (2009). In most models, the simulation of the highest intensity of the heat band in the winter season extends south of 4° S, with intensities greater than 6 °C in some models, though, intensities simulated by GISS-ESM-E2-1G and MRI-ESM2-0 are less than 5 °C.

During spring (MAM), the heat band narrows (lying between latitudes 8°N and 20°N) with highest intensities similar to that of the winter season. In CNRM-CM6-1, MPI-ESM1-2-HR and MPI-ESM1-2-LR (GISS-ESM-E2-1G, IPSL-CM6A-LR, MPI-ESM1-2-HAM and NorESM2-LM) the width of the WAHB is slightly thicker (thinner) than that of the references. Also, highest intensities are slightly weaker in models such as GISS-ESM-E2-1G, IPSL-CM6A-LR, and NorESM2-LM, than the references, whereas models including MPI-ESM1-2-HR and MPI-ESM1-2-LR simulate the highest intensities of the WAHB between 6 and 7 °C.

The summer season (JJA) has the highest intensities of the heat band and the northernmost location of the WAHB. The results of the WAHL in the previous section of this study and also other studies (e.g., Drobinski et al. 2005; Ramel et al. 2006; Lavaysse et al. 2009; Dixon et al. 2017) indicate that the strongest heat low core which occurs in July and August is located over the Sahara. This is consistent to the WAMS. There are some uncertainties in the representation of the seasonal zonal WAHB in the reference datasets. All the 8 CMIP6 models used in this study fairly represented the location of the zonal heat band however, the highest intensities are simulated differently. For instance, highest intensities are stronger (weaker) than the references in models such as GISS-ESM-E2-1G, MPI-ESM1-2-HR and MRI-ESM2-0 (CNRM-CM6-1, IPSL-CM6A-LR, MPI-ESM1-2-HAM and NorESM2-LM). It is interesting to note that among the 3 models that simulate strongest intensities of the zonal WAHB in the summer season, only GISS-ESM-E2-1G simulates a corresponding stronger heat low core in July and August in comparison to the reanalysis products.



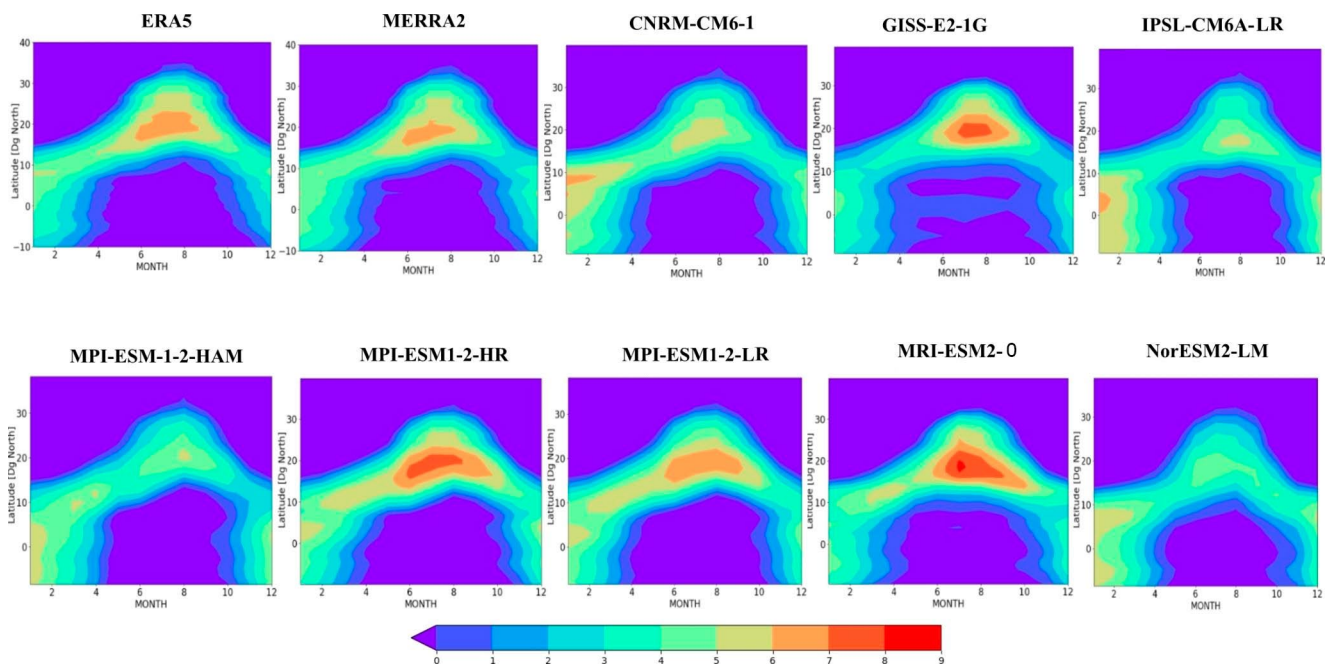


**Fig. 4** Hovmoeller diagram (from 25° W to 30° E) of the climatological (1983–2012) monthly mean of the WAHB. The colour bar shows zonal heat band intensity (near surface temperature) in °C

The highest intensities simulated by the MPI-ESM1-2-LR are similar to that of the references.

In the autumn season (SON), the zonal WAHB retreats to the south with highest intensities between 2 and 6 °C according to both references. The differences in the simulated highest intensities and the location of the autumn zonal heat band by the models are within the range of the reference datasets.

### 3.3 West African Rain Band

#### 3.3.1 Spatial structure of the WARB

In January and February, the WARB lies south of 8°N (5°N) over the ocean (continent), with total monthly precipitation greater than 135 mm over the ocean (continent) in the western (eastern) parts of the domain in the GPCP dataset (Fig. 5). The WARB is located southward of both the WAHB and the WAHL. In these months dry conditions prevail over the whole West African region which is consistent with the location of the ITCZ (below 5°N) (Sultan and Janicot 2003). MRI-ESM2-0 simulates a stronger and thicker rain band than GPCP over both ocean and continent, with the location of the WARB further south than that of the reference over the ocean, but with similar location as the reference over the continent. The simulations by CNRM-CM6-1, GISS-ESM-E2-1G are stronger/thicker (weaker) than the reference over the ocean (continent). In the case of the CNRM-CM6-1 simulation, there is a second rain band

located below latitude 0° over the ocean (this second WARB over the ocean is also simulated in NorESM2-LM, IPSL-CM6A-LR). The GISS-ESM-E2-1G model locates the rain band over the ocean below latitude 0°, which is also the location of WARB simulated by all the 3 MPI models over both ocean and continent. Intensities are weaker in both NorESM2-LM, IPSL-CM6A-LR simulations over ocean and continent than in GPCP. On the other hand, intensities are stronger/thicker over the ocean, but thinner over the continent than GPCP in the MPIs' simulation.

There is a slight northwards extension and a widening of the WARB from March to April. These are the rainfall onset months for the Guinea Coast sub-region (Sultan and Janicot 2003; Annor et al. 2018; Agyekum et al. 2018) over West Africa. The rain band is located in the southern parts of West African coastal countries, close to 5°N, and this location is also similar to that of the ITCZ in April. All the 8 models simulated the WARB at a lower latitude than GPCP over the ocean, whereas, models like MRI-ESM2-0, NorESM2-LM, IPSL-CM6A-LR and GISS-ESM-E2-1G simulate the location of the rain band quite similarly to that of the reference dataset over the continent. Model such as CNRM-CM6-1 and GISS-ESM-E2-1G, simulate a stronger and wider (weaker and thinner) rain band over the ocean (continent) compared to GPCP. Whereas the MRI-ESM2-0 and all the MPI models simulate a stronger and wider rain band, especially over the ocean, than the reference. The NorESM2-LM model simulates slightly weaker WARB than GPCP, whereas the simulation of the intensity by IPSL-CM6A-LR

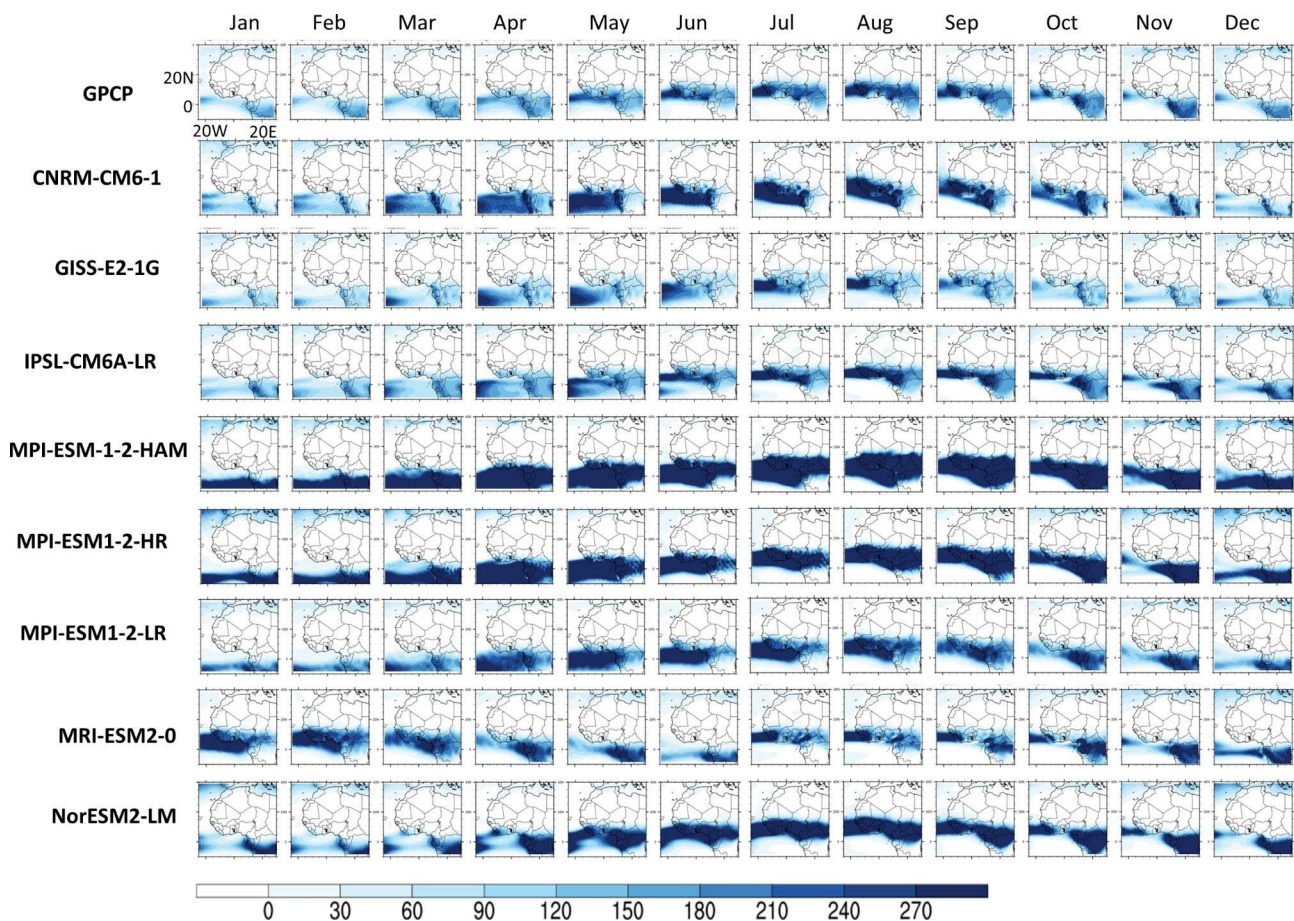


**Fig. 5** Maps of monthly total WARB for the 1983–2012 climatological period for the reference and the 8 CMIP6 GCMs. The colour bar shows rain band intensity (total monthly rainfall) in mm

is quite similar to the reference dataset over the continent. The results imply that the simulation of the northward migration of the ITCZ in the models could be slower than the reference dataset; which could in turn imply that March and April may not be captured as the onset of the rainy season over the Guinea Coast by the models. This assertion, to some extent, is confirmed in the simulations by the models, where barely any of the WARBs are located over the Guinea Coast during these months.

In May and June, there is still a further northwards progression of the WARB. This is the first rainy season for the Guinea Coast sub-region, whereas the Soudano-Sahel and the Sahel in West Africa receive the onset of the rainfall (Sultan and Janicot 2003; Sylla et al. 2009; Annor et al. 2018; Agyekum et al. 2018). Again, the location of the WARB is consistent with that of the ITCZ reported by Sultan and Janicot (2003). In May and June, highest intensity heat bands are located between  $10^{\circ}\text{N}$  and  $30^{\circ}\text{N}$ , with the location of the rain band at the transition zone (between  $0^{\circ}$  and  $10^{\circ}\text{N}$ ) of the latitudinal temperature gradient over the region, confirming the pulling of moisture onto the continent by the northward movement of the latitudinal temperature

gradient. Models such as CNRM-CM6-1 and GISS-ESM-E2-1G are not able to reproduce the GPCP's rain band over the continent especially in the eastern parts of the domain. The northwards migration of the WARB in the models is quite normal over the land, but a bit slower over the ocean. The highest intensities of rain band over the Guinea Coast are captured quite well by most of the models.

A further migration of the WARB to the northernmost location is seen in the reference dataset in July and August. The highest intensities of the rain band are broadened over the continent from the central to the eastern parts of the region. The middle of the rain band moves to around  $10^{\circ}\text{N}$  which is consistent with the location of the ITCZ according to Sultan and Janicot (2003). Also, the very low intensity WARB over the Guinea Coast zone between  $10^{\circ}\text{W}$  and  $5^{\circ}\text{E}$  is consistent with the abrupt shift of the ITCZ between the same longitudes, as reported by Sultan and Janicot (2003). In these months, areas in the Guinea Coast zone between  $10^{\circ}\text{W}$  and  $5^{\circ}\text{E}$  enter into the so-called little dry season, hence the very low intensity WARB seen in the GPCP data. On the other hand, the Soudano-Sahel and the Sahel receive most of their annual rainfall in these months which is clearly shown

by the location of the highest intensity of the WARB. Models such as MRI-ESM2-0, NorESM2-LM, IPSL-CM6A-LR and MPI-ESM1-2-HR simulate the intensity, location and the size of the WARB quite close to GPCP, though the little dry season feature over the Guinea Coast is missing, except in NorESM2-LM. In the CNRM-CM6-1 model, stronger (weaker) intensity and faster (slower) northwards rain band migration are simulated over the half western (eastern) parts of the domain compared to GPCP. The difficulty found in CNRM-CM6-1's pulling of the moisture over the continent especially in the east, could be linked to the weak latitudinal temperature gradient simulated by this model (see Fig. 3 and Hagos and Cook 2007; Hsieh and Cook 2008; Dixon et al. 2017). GISS-ESM-E2-1G captures quite well the location of the rain band, but the intensity is weaker over the continent. MPI-ESM-1-2-HAM and MPI-ESM1-2-LR both simulate slightly stronger intensity and slower northward migrating WARBS, especially over the ocean.

The September WARB has a similar pattern to August, but it retreats southwards to quite a similar location to the rain band in June. The highest intensities of the WARB cover the entire region from the Guinea Coast to the Sahel. September (like June) is the peak month for the second rainy season over the Guinea Coast, which is in agreement with the GPCP rain band result. The October WARB has a similar pattern as the one in May, however, from 10°W to the east, there is virtually no rain band over the ocean. The rain band is found in the Guinea Coast and the southern parts of the Soudano-Sahel sub-regions. The simulations for both months are quite close to the reference dataset in models such as MRI-ESM2-0, NorESM2-LM, IPSL-CM6A-LR, GISS-ESM-E2-1G, MPI-ESM1-2-HR and MPI-ESM1-2-LR. The CNRM-CM6-1 model on the other hand simulates a stronger, wider and a slower southward migrating WARB in the west, with barely no/low intensity rain band in the eastern corner. The simulation of the WARB by the MPI-ESM-1-2-HAM model is slightly stronger and wider over both ocean and continent than the GPCP's WARB.

In November and December, the WARB migrates to the southernmost location, with patterns similar to that in January and February. In these months, the ITCZ is in its southernmost location (in conformity with the WARB in the GPCP), marking the beginning of the major dry season over West Africa. The migration of the WARB is simulated faster by models including MRI-ESM2-0, CNRM-CM6-1, GISS-ESM-E2-1G and all the MPI models in order to locate the WARB at lower latitudes than GPCP. The intensity simulations are slightly stronger over both ocean and continent in the MRI-ESM2-0, IPSL-CM6A-LR, MPI-ESM-1-2-HAM, MPI-ESM1-2-HR and MPI-ESM1-2-LR models. Whereas, the intensity is slightly weaker (stronger) over the continent (ocean) in models such as CNRM-CM6-1 and

GISS-ESM-E2-1G. The NorESM2-LM model simulates a thinner WARB, especially over the ocean, compared to the reference dataset.

### 3.3.2 Zonal structure of WARB

In Fig. 6, we have indicated the climatological monthly mean time-latitude Hovmoeller diagrams of the WARB for all the datasets, showing the seasonal cycle of the rain band over the West African region.

In the dry season (November- February) the highest intensity of the rain band (75-100 mm) is similar for all of the dry season months, with the middle of the zonal rain band mostly around latitude 0° according to Fig. 6. This result is consistent with the location of the ITCZ over the region in the dry season. During this season, almost the entire West African region is under the influence of the dry, dusty northeast trade winds, forcing the convergence zone to the southernmost location (Sultan and Janicot 2003; Sylla et al. 2009; Annor et al. 2018; Agyekum et al. 2018). All the 8 CMIP6 models overestimate the GPCP's precipitation, however, models such as CNRM-CM6-1, GISS-ESM-E2-1G and IPSL-CM6A-LR simulate the highest intensity relatively closer to that of the reference dataset for some months in the season. Also, all the models locate the middle of the zonal rain band at latitudes further south than 0°. With the exception of the GISS-ESM-E2-1G model (which is one of the models with highest intensity relatively close to the reference), all the models simulate stronger highest zonal heat band intensities than the references (see Fig. 4), and the highest intensities are also located at lower latitudes compared to the references. Therefore, the stronger highest intensities of the zonal WARB; that are located south of latitude 0° in the models could be linked to the simulations of stronger temperature gradient at the transition zone of the ocean and the continent. This result is in agreement with several studies including Hagos and Cook (2007), Hsieh and Cook (2008), Dixon et al. (2017).

In the wet season months the highest zonal WARB intensities increase from 100 mm in March, to greater than 150mm in August (when northernmost location of zonal rain band is reached). By October, the highest intensity decreases below 150 mm and the zonal WARB returns to the south. The simulations of the intensities of the rain band in the onset (March) and cessation (October) months are stronger in the models, though GISS-ESM-E2-1G and IPSL-CM6A-LR (CNRM-CM6-1) simulate intensities relatively closer to that of GPCP for both March and October (only October). Most of the models simulate wider highest intensity zonal WARBS than GPCP. On the other hand, the level of the highest intensity (greater than 150 mm) and the northernmost location of the zonal rain band in the wet

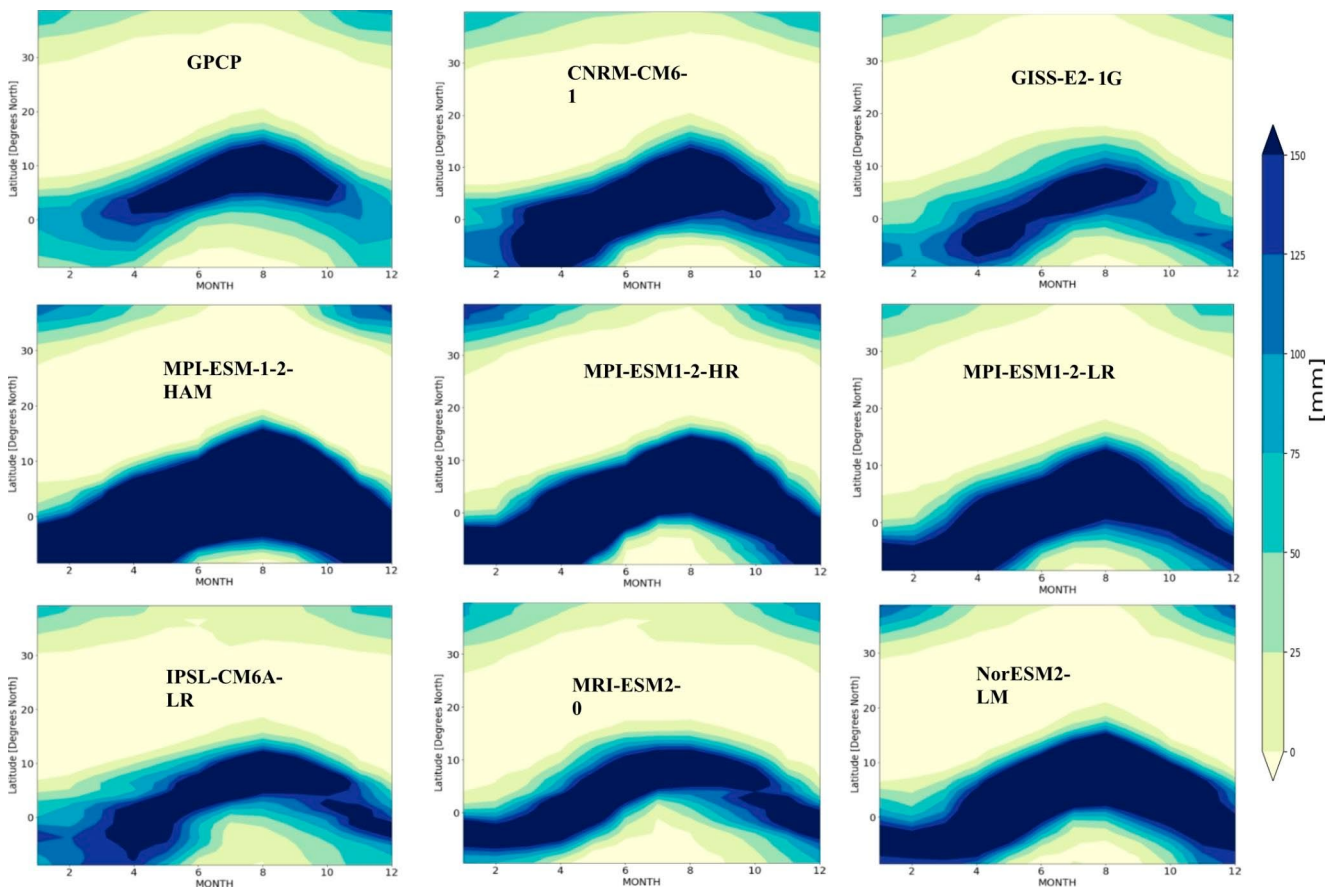


**Fig. 6** Hovmoeller diagram (from 25° W to 30° E) of the climatological (1983–2012) monthly mean of the WARB (mm). The colour bar shows zonal rain band intensity (total monthly rainfall) in mm

season are reasonably captured by the models. It worth mentioning that the northernmost location of the zonal rain band in the wet season in the models' simulations in general are at lower latitudes than the reference. The dynamics (i.e., the north-south migration) of the zonal rain band in the wet season over the region, are quite well represented, though a bit slower in the models. This implies that the models are simulating an ITCZ that is located at lower latitudes than observed. The results presented here are consistent with Dixon et al. (2017) which shows that models with northward Sahara Heat Low biases have enhanced short wave absorption and increased low-level specific humidity (see their Fig. 5) through the development of the Saharan water vapor–temperature feedback (as described in Evan et al. (2015)). In the case of this study, slightly southward biases are seen in the models' simulations of the WAHL and the WAHB, which could be the possible reason for the southward biases in the simulation of the WARB by the models.

### 3.4 Differences in the simulations of the three features in relation to each GCM's specification

The simulations of climate variables in GCMs are impacted by several factors. Notable among them are the resolution and parameterization. This section discusses how these two factors could contribute to the differences in the simulations of the WAHL, WAHB and the WARB by the models. The main target of both a high-resolution simulation and a parameterization in climate models is to resolve small-scale features in order to represent the heterogeneities that exist in grid (i.e., high resolution) and sub-grid (parameterization) levels.

All the 8 GCMs used in the study have atmosphere (highest resolution being 100 km for MPI-ESM1-2-HR and MRI-ESM2-0 and the lowest resolution at 250 km for rest of the models), land (the same as atmosphere), ocean (the highest resolution at 50 km for MPI-ESM1-2-HR and the lowest at 250 for MPI-ESM1-2-LR and MPI-ESM1-2-HAM, with the rest having 100 km resolution) and sea ice (again the MPI-ESM1-2-HR has the highest resolution of 50 km, GISS-E2-1G, MPI-ESM1-2-LR and MPI-ESM1-2-HAM

have the lowest of 250 and the rest at 100 km resolution) components. Except the NorESM2-LM model at 250 km resolution, all the rest of the models do not have a land ice component. The ocean biogeochemical component is present at resolutions ranging from 50 to 250 km, but CNRM-CM6-1 and GISS-E2-IG have no ocean biogeochemical component. IPSL-CM6A-LR, MPI-ESM1-2-HR and MPI-ESM1-2-LR do not have atmospheric chemistry, but the rest of the models have it at 250 km resolution. With the exception of IPSL-CM6A-LR (none) and MPI-ESM1-2-HR (at 100 km), the rest of the GCMs have an aerosol component at 250 km. The GCM with all the 8 components is the NorESM2-LM and the one with the least (5 components) is the IPSL-CM6A-LR model. In terms of resolution, the MPI-ESM1-2-HR (MPI-ESM-1-2-HAM) has the highest (lowest) resolution in all the components that are incorporated in the development of the model (Voldoire et al. 2018; NASA, 2018; Boucher et al. 2018; Jungclaus et al. 2019; Wieners et al. 2019; Neubauer et al. 2019; Yukimoto et al. 2019; Seland et al. (2019).

Among the 8 components that are incorporated in the development of the models, paramount to the representation of the WAHL are the atmosphere, land and ocean, although aerosol and atmospheric chemistry could impact the representation through radiative forcing of the formation of chemical compounds that are radiatively active. The LLAT is impacted strongly by the mean temperature between the 925 and the 700 hPa levels and therefore requires that ocean-land-atmosphere processes responsible for mean temperature between these two pressure levels are appropriately resolved in the models. Also, the westward movement of the WAHL from January to August which has been attributed to the leeward depression of the Aïr and Hoggar mountains (Semazzi and Sun 1997; Drobinski et al. 2007; Lavaysse et al. 2009), could require a climate model with adequate resolution and parameterization that could resolve the leeward depression of these mountains. From Fig. 2, it is only the GISS-E2-IG model which has a stronger core intensity WAHL than the reanalysis datasets. The rest of the models have weaker core intensity WAHL for the JJAS months. For the NDJFM months, almost all the models have stronger core intensity WAHL than the reanalysis datasets. This suggests that though resolution might play a role, the differences in the representation of WAHL by the GCMs could be attributed to the kind of parameterization in the models, since the model with the highest resolution (MPI-ESM1-2-HR) could not simulate the WAHL so differently from its low-resolution counterparts MPI-ESM1-2-LR and MPI-ESM-1-2-HAM. This assertion is corroborated in the way the CNRM-CM6-1 model simulates the WAHL, especially for the JJAS months.

Similarly, the simulation of the WAHB by the models could more significantly be influenced by the parameterization than resolution. Models such as GISS-E2-IG, MPI-ESM1-2-HR and MRI-ESM2-0 (CNRM-CM6-1, IPSL-CM6A-LR, MPI-ESM-1-2-HAM and NorESM2-LM) with different resolutions simulate stronger (weaker) JJAS WAHB than the reanalysis datasets. Different parameterization schemes in the models that are responsible for the partitioning of incoming solar radiation into sensible heat and latent heat over the continent and the ocean could be responsible for the differences in the simulation of the WAHB. As pointed out earlier, surface heating increases the thickness of the PBL, thereby, influencing the representations of both the WAHB and WAHL by the models which is highly controlled by the surface heating as reported by Drobinski et al. (2005), Lavaysse et al. (2009) and Dixon et al. (2017).

In the case of the WARB, parameterization schemes handling mesoscale convective activities in the models could be responsible for the differences in the simulations of the rain band. Over the West African region, mesoscale convective activities (which are influenced by model resolution) play a significant role in precipitation processes. Another synoptic feature influencing West African precipitation is the influx of moisture from the ocean to the land especially in the summer monsoon (Annor et al. 2018, 2022; Agyekum et al. 2018). A look at the simulations of the WARB shows that these two factors are represented differently in the models. For instance, the simulation of the WARB by CNRM-CM6-1 could be attributed to the model's inability to pull the moisture flux on the land. In the case of the 3 MPI models (and also, the rest of the models), resolution of the models could be the reason for the difference in the simulation of the rain band. The representation of the WARB by the MPI-ESM1-2-HR model (the model with the highest resolutions in all the applied climate components in the model development) is relatively closer to that of the reference dataset than the rest (especially the MPI-ESM1-2-LR and MPI-ESM-1-2-HAM which have similar (coarser) resolutions for the applied climate components in their development). Models such as GISS-E2-IG, IPSL-CM6A-LR, MRI-ESM2-0 and NorESM2-LM simulate the rain band relatively better than the MPI-ESM1-2-LR and MPI-ESM-1-2-HAM suggesting the influence of model resolution on the representation of the WARB by the models.

## 4 Summary and conclusions

In this study, datasets, including reanalysis products and a satellite-gauge merged dataset, have been applied to demonstrate the climatological annual cyclical movement of the

WAMS in three components, namely, the WAHL, WAHB and the WARB. We have also evaluated the performance of 8 CMIP6 GCMs in reproducing the climatological annual migration of these three features over the same domain. Geopotential height fields spanning 1983–2012 were extracted from ERA-Interim and ERA5 as references and the 8 models in the investigation of the annual migration of the WAHL, applying the LLAT approach. Also, for the WAHB, 2-m air temperature outputs from two reanalysis products (ERA5 and MERRA2) and the 8 CMIP6 models were used for the same period and domain. The GPCP precipitation dataset is used as a reference dataset for the evaluation of the WARB for the 8 models.

In general, all the GCMs are able to reproduce the climatological monthly migration of the WAHL found in the reanalysis datasets, however the location of the WAHL in August simulated by the CNRM-CM6-1 model extends further east of the Sahel region, and in the case of the MPI models a smaller secondary heat low is located in the eastern part of the Sahara. Most of the models simulate generally stronger intensities than the references for the dry season (winter) months (November–March) and weaker intensities for the wet season (summer) months (May to August), with the exception of GISS-E2-IG (MRI-ESM2-0) which simulates generally slightly stronger (weaker) intensities than the references for all months.

The monthly dynamics of the WAHB are similar to that of the WAHL. Also, the results show that the WAHB has higher intensities over the continent than the ocean. These similar dynamics in both the WAHL and the WAHB could be linked to the annual cyclical migration of incoming shortwave radiation, which has also been reported in earlier studies including Drobinski et al. (2005), Lavaysse et al. (2009) and Dixon et al. (2017). There is an overestimation of the WAHB's spatial intensity mostly over the ocean by the models in general. The models simulate the migration of the zonal heat band for all months fairly well, however models such as GISS-E2-IG, MPI-ESM1-2-HR and MRI-ESM2-0 (CNRM-CM6-1, IPSL-CM6A-LR, MPI-ESM1-2-HAM and NorESM2-LM) overestimated (underestimate) the summer months' heat band intensities.

Similar to the WAHL and the WAHB, the WARB migrates from the southernmost location in January, reaches the northernmost location in August, and then migrates to the southernmost location in December. All the models fairly represented the annual cycle of the monthly WARB dynamics (changes in location and intensity). However, most of the models simulate the rain band at lower latitudes (southward biases) than GPCP and also the intensities are weaker (stronger) over the continent (ocean) in the simulations, especially in the CNRM-CM6-1 and GISS-E2-IG models. All the 8 CMIP6 models overestimate GPCP's highest

intensity of the zonal rain band in the dry season months, however, models such as CNRM-CM6-1, GISS-ESM-E2-1G and IPSL-CM6A-LR simulate the highest intensity relatively closer to that of the reference dataset for some months in the season. The simulations of the intensities of the rain band in the onset (March) and cessation (October) months are also stronger in the models. The location of the zonal rain band in both wet and dry seasons in the models' simulations in general are further south than the reference, implying the simulation of an ITCZ that is located further south than observed.

We have elucidated the close linkages between the West Africa Heat Low, Heat Band and the Rain Band as signature components of the WAMS in their climatological annual dynamics. We have also shown that all the features migrate from the south (with the minimum intensities) in January to the north (with the maximum intensities) in August over the region. All the 8 GCMs applied in the study are able to represent the climatological annual dynamics of all the three features and the linkages between them indicating the satisfactory representation of the WAMS in the 8 CMIP6 models in general, though, difference in the models' simulations of these features exist, which is also true in the case where more than one reference dataset is applied. Our results are in agreement with earlier studies (e.g., Vizy and Cook 2009; Chauvin et al. 2010; Lavaysse et al. 2010a) that show that the import of moisture and sensible heat into the northern Sahara through the midlatitude jet have impact on the Sahara Heat Low on a synoptic scale. It is also important to mention the weaknesses in the models' simulations – which are in general weaker intensities of heat low and slightly southward biases in the locations of the three features, particularly in the case of the WAHB and the WARB. These weaknesses in the simulations by the models are also consistent with Dixon et al. (2017). Our study suggests that the model evaluation process can be applied for the future investigation of these features in order to develop appropriate warning systems for any future changes that might occur. Also, model developers can utilize the outcome of this study to highlight model development that is targeted at the improvement of these features as key components of the WAMS.

**Acknowledgements** This work has been conducted for the Foreign Commonwealth and Development Office (FCDO)-funded LaunchPAD (Priority on African Diagnostics) project, part of the Future Climate for Africa (FCFA) program (futureclimateafrica.org). We gratefully acknowledge the funding of this work. The authors are thankful to the staff members of the JASMIN High Performance Computing System for making this system available for data access and analysis. We acknowledge the usefulness of all the reference datasets including ERA-Interim and ERA5 from the ECMWF, MERRA2 from NASA, and the producers of the GPCP data. We acknowledge the World Climate Research Programme, which, through its Working Group on Coupled Modelling, coordinated and promoted CMIP6. We

thank the climate modeling groups for producing and making available their model output, the Earth System Grid Federation (ESGF) for archiving the data and providing access, and the multiple funding agencies who support CMIP6 and ESGF.

**Author contributions** All authors contributed to the study conception and design. Material preparation, data collection and analysis were performed by Thompson Annor, Apphia Tetteh Ackon, Rachel James, Ellen Dyer and Thomas Webb. The first draft of the manuscript was written by Thompson Annor and all authors commented on previous versions of the manuscript. All authors read and approved the final manuscript.

**Funding** This work was supported by the UK Foreign Commonwealth and Development Office (formerly the Department for International Development), as part of the LaunchPAD project, under the Future Climate for Africa consortium.

**Data availability** The model output data sets used in this study were made available through the Earth System Grid Federation (ESGF) Peer-to-Peer system (<https://data.ceda.ac.uk/badc/cmip6/>). Reanalysis data used in this analysis were provided by the Copernicus Climate Change Service (<https://cds.climate.copernicus.eu/cdsapp#!> home; Hersbach et al. 2020), ECMWF (<https://ecmwf.int/en/forecasts/datasets/reanalysis-datasets/era-interim>) and NASA (<https://disc.sci.gsfc.nasa.gov/daac-bin/FTPSubset.pl>). The authors' code is available online ([https://github.com/Priority-on-African-Diagnostics/LaunchPAD/West\\_African\\_Heat\\_Low\\_Rain\\_Band\\_Heat\\_Band](https://github.com/Priority-on-African-Diagnostics/LaunchPAD/West_African_Heat_Low_Rain_Band_Heat_Band)).

## Declarations

**Competing interests** The authors declare no competing interests.

**Conflict of interest** The authors declare that they have no conflicts of interest.

**Ethics approval** Not applicable.

**Consent to participate** Not applicable.

**Consent for publication** Not applicable.

**Open Access** This article is licensed under a Creative Commons Attribution 4.0 International License, which permits use, sharing, adaptation, distribution and reproduction in any medium or format, as long as you give appropriate credit to the original author(s) and the source, provide a link to the Creative Commons licence, and indicate if changes were made. The images or other third party material in this article are included in the article's Creative Commons licence, unless indicated otherwise in a credit line to the material. If material is not included in the article's Creative Commons licence and your intended use is not permitted by statutory regulation or exceeds the permitted use, you will need to obtain permission directly from the copyright holder. To view a copy of this licence, visit <http://creativecommons.org/licenses/by/4.0/>.

## References

Adler RF, Sapiano M, Huffman GJ, Wang J-J, Gu G, Bolvin D, Chiu L, Schneider U, Becker A, Nelkin E, Xie P, Ferraro R, Shin D-B (2018) The global precipitation Climatology Project (GPCP) monthly analysis (New Version 2.3) and a review of 2017 global

- precipitation. *Atmosphere* 9(4):138. <https://doi.org/10.3390/atmos9040138>
- Agyekum J, Annor T, Lamptey B, Quansah E, Agyemang RYK (2018) Evaluation of CMIP5 global climate models over the Volta Basin: precipitation. *Adv Meteorol* 2018:1–25
- Akinsanola AA, Ajayi VO, Adejare AT, Adeyeri OE, Gbode IE, Ogunjobi KO, Nikulin G, Abolude AT (2017) Evaluation of rainfall simulations over West Africa in dynamically downscaled CMIP5 global circulation models. *Theor and Appl Climatol* 15. <https://doi.org/10.1007/s00704-017-2087-8>
- Annor T, Lamptey B, Wagner S, Oguntunde P, Arnault J, Heinzeller D, Kunstmann H (2018) High-resolution long-term WRF climate simulations over Volta Basin. Part 1: validation analysis for temperature and precipitation. *Theor and Appl Climatol* 144(3–4):829–849
- Annor T, Lamptey B, Washington R (2022) Assessment of the unified model in reproducing west african precipitation and temperature climatology. *Theoret Appl Climatol* 148(1):779–794. <https://doi.org/10.1007/s00704-022-03973-1>
- Berrisford P, Dee DP, Poli P, Brugge R, Fielding M, Fuentes M, Källberg PW, Kobayashi S, Uppala S, Simmons A (2011) The ERA-Interim archive Version 2.0 ERA Report Series, ECMWF, Shinfield Park, Reading. <https://www.ecmwf.int/node/8174>
- Biasutti M (2019) Rainfall trends in the african sahel: characteristics, processes and causes. *Wiley Interdisciplinary Reviews, Climate Change*, e591
- Boucher O, Denvil S, Levvasseur G, Cozic A, Caubel A, Foujols M-A, Meurdesoif Y, Cadule P, Devilliers M, Ghattas J, Lebas N, Lurton T, Mellul L, Musat I, Mignot J, Cheruy F (2018) IPSL IPSL-CM6A-LR model output prepared for CMIP6 CMIP historical. Version 2021. <https://doi.org/10.22033/ESGF/CMIP6.5195>. Earth System Grid Federation
- Chauvin F, Roehrig R, Lafore J-P (2010) Intraseasonal variability of the Saharan heat low and its link with midlatitudes. *J Clim* 23:2544–2561. <https://doi.org/10.1175/2010JCLI3093.1>
- Dixon RD, Daloz AS, Vimont DJ (2017) Saharan Heat Low Biases in CMIP5 models. *J Clim* 30(8):2867–2884. <https://doi.org/10.1175/JCLI-D-16-0134.1>
- Drobinski P, Sultan B, Janicot S (2005) Role of the Hoggar massif in the west african monsoon onset. *Geophys Res Lett* 32L01705. <https://doi.org/10.1029/2004GL020710>
- Drobinski P, Bastin S, Janicot S, Dabas A, Delville P, Reitebuch O (2007) Role of scale interactions and orography on the late northward propagation of the west african monsoon in summer 2006 in the region of Niger/Mali. in revision in *J Geophys Res*
- Evan AT, Flamant C, Lavaysse C, Kocha C, Saci A (2015) Water vapor–forced greenhouse warming over the Sahara Desert and the recent recovery from the Sahelian drought. *J Clim* 28:108–123. <https://doi.org/10.1175/JCLI-D-14-00039.1>
- Eyring V, Bony S, Meehl GA, Senior CA, Stevens B, Stouffer RJ, Taylor KE (2016) Overview of the Coupled Model Intercomparison Project Phase 6 (CMIP6) experimental design and organization. *Geoscientific Model Development* 2016, 9, 1937–1958
- Gu G, Adler RF (2004) Seasonal evolution and variability associated with the west african monsoon system. *J Clim* 17(17):3364–3377
- Hagos SM, Cook KH (2007) Dynamics of the West Africa monsoon jump. *J Clim* 20(1):5264–5284
- Hersbach H, Bell B, Berrisford P, Hirahara S, Horányi A, Muñoz-Sabater J, Nicolas J, Peubey C, Radu R, Schepers D et al (2020) The era5 global reanalysis. *Q J R Meteorol Soc* 146(730):1999–2049
- Hsieh J-S, Cook KH (2008) On the instability of the african easterly jet and the generation of african waves: reversals of the potential vorticity gradient. *J Atmos Sci* 65:2130–2151. <https://doi.org/10.1175/2007JAS2552.1>

- Jung G, Kunstmann H (2007) High-resolution regional climate modeling for the Volta region of West Africa. *J Geophys Res* 112:D23108. <https://doi.org/10.1029/2006JD007951>
- Jungclaus J, Bittner M, Wieners K-H, Wachsmann F, Schupfner M et al (2019) MPI-M MPI-ESM1.2-HR model output prepared for CMIP6 CMIP historical. Version 2021. <https://doi.org/10.22033/ESGF/CMIP6.6594>. Earth System Grid Federation
- Klein C, Heinzeller D, Bliefemicht J, Kunstmann H (2015) Variability of west african monsoon patterns generated by a WRF multi physics ensemble. *Clim Dyn*. <https://doi.org/10.1007/s00382-015-2505-5>
- Lavaysse C, Flamant C, Janicot S, Parker DJ, Lafore J-P, Sultan B, Pelon J (2009) Seasonal evolution of the west african heat low: a climatological perspective. *Clim Dyn* 33:313–330. <https://doi.org/10.1007/s00382-009-0553-4>
- Lavaysse C, Flamant C, Janicot S (2010a) Regional-scale convection patterns during strong and weak phases of the Saharan heat low. *Atmos Sci Lett* 11(4):255–264
- Lavaysse C, Flamant C, Janicot S, Knippertz P (2010b) Links between african easterly waves, midlatitude circulation and intraseasonal pulsations of the west african heat low. *Q J R Meteorol Soc* 136(S1):141–158
- Lavaysse C, Flamant C, Evan A, Janicot S, Gaetani M (2016) Recent climatological trend of the Saharan heat low and its impact on the west african climate. *Clim Dyn* 47:3479–3498. <https://doi.org/10.1007/s00382-015-2847-z>
- Mariotti L, Coppola E, Sylla MB, Giorgi F, Piani C (2011) Regional climate model simulations of projected 21st century climate change over an all-Africa domain: comparison analysis of nested and driving model results. *J Geophys Res Atmos* 116(D15):16
- Marshall J, Donohoe A, Ferreira D, McGee D (2014) The ocean's role in setting the mean position of the inter-tropical convergence zone. *Clim Dyn* 42(7–8):1967–1979
- McCrary RR, Randall DA, Stan C (2014) Simulations of the west african monsoon with a Superparameterized Climate Model. Part I: the Seasonal cycle. *J Clim* volume 27:8303–8322. <https://doi.org/10.1175/JCLI-D-13-00676.1>
- NASA/GISS (2018) NASA-GISS (Goddard Institute for Space Studies) GISS-E2.1G model output prepared for CMIP6 CMIP historical. Version 2021. <https://doi.org/10.22033/ESGF/CMIP6.7127>. Earth System Grid Federation
- Neubauer D, Ferrachat S, Siegenthaler-Le Drian C, Stoll J, Folini DS et al (2019) HAMMOZ-Consortium MPI-ESM1.2-HAM model output prepared for CMIP6 CMIP historical. Version 2021. <https://doi.org/10.22033/ESGF/CMIP6.5016>. Earth System Grid Federation
- Okafor G, Annor T, Odai S, Agyekum J (2019) Volta basin precipitation and temperature climatology: evaluation of CORDEX-Africa regional climate model simulations. *Theor and Appl Climatol* 137(3–4):2803–2827
- Ramel R, Gallée H, Messager C (2006) On the northward shift of the west african monsoon. *Clim Dyn* 26:429–440. <https://doi.org/10.1007/s00382-005-0093-5>
- Rienecker MM, Suarez MJ, Gelaro R, Todling R, Bacmeister J, Liu E, Bosilovich MG, Schubert SD, Takacs L, Kim GK, Bloom S, Chen J, Collins D, Conaty A, Da Silva A, Gu W, Joiner J, Koster RD, Lucchesi R, Molod A, Owens T, Pawson S, Pegion P, Redder CR, Reichle R, Robertson FR, Ruddick AG, Sienkiewicz M, Woollen J (2011) MERRA: NASA's Modern-Era Retrospective Analysis for Research and Applications. *J Clim* 24:3624–3648. <https://doi.org/10.1175/JCLI-D-11-00015.1>
- Seland Ø, Bentsen M, Olivie DJL, Toniazzo T, Gjermundsen A et al (2019) NCC NorESM2-LM model output prepared for CMIP6 CMIP historical. Version 2021. <https://doi.org/10.22033/ESGF/CMIP6.8036>. Earth System Grid Federation
- Semazzi FHM, Sun L (1997) The role of orography in determining the Sahelian climate. *Int J of Climatol* 17:581–596
- Sultan B, Janicot S (2003) The west african Monsoon dynamics. Part II: the “preonset” and “onset of the summer monsoon. *J Clim* 16(21):3407–3427
- Sylla MB, Gaye AT, Pal JS, Jenkins GS, Bi XQ (2009) High-resolution simulations of west african climate using regional climate model (RegCM3) with different lateral boundary conditions. *Theor Appl Climatol* 98:293–314. <https://doi.org/10.1007/s00704-009-0110-4>
- Thorncroft C, Blackburn M (1999) Maintenance of the african easterly jet. *Quart J Roy Meteor Soc*, (125): 763–786
- Vellinga M, Roberts M, Vidale PL, Mizieliński MS, Demory M-E, Schiemann R, Strachan J, Bain C (2016) Sahel decadal rainfall variability and the role of model horizontal resolution. *Geophys Res Lett* 43:326–333. <https://doi.org/10.1002/2015GL066690>
- Vigaud N, Roucou P, Fontaine B, Sijikumar S, Tyteca S (2011) WRF/ARPEGE-CLIMAT simulated climate trends over West Africa. *Clim Dyn* (36):925–944
- Vizy EK, Cook KH (2009) A mechanism for african monsoon breaks: Mediterranean cold air surges. *J Geophys Res* 114D01104. <https://doi.org/10.1029/2008JD010654>
- Voldoire A et al (2018) CMIP6 simulations of the CNRM-CERFACS based on CNRM-CM6-1 model for CMIP experiment historical. Version 2021. <https://doi.org/10.22033/ESGF/CMIP6.4066>. Earth System Grid Federation
- Wieners K-H, Giorgetta M, Jungclaus J, Reick C, Esch M et al (2019) MPI-M MPI-ESM1.2-LR model output prepared for CMIP6 CMIP historical. Version 2021. <https://doi.org/10.22033/ESGF/CMIP6.6595>. Earth System Grid Federation
- Yukimoto S, Koshiro T, Kawai H, Oshima N, Yoshida K et al (2019) MRI MRI-ESM2.0 model output prepared for CMIP6 CMIP historical. Version 2021. Earth System Grid Federation. <https://doi.org/10.22033/ESGF/CMIP6.6842>
- Zuidema P, Chang P, Medeiros B, Kirtman BP, Mechoso R et al (2016) Challenges and prospects for reducing coupled climate model SST biases in the Eastern Tropical Atlantic and Pacific Oceans. *BAMS* 2016:2305–2328. <https://doi.org/10.1175/BAMS-D-15-00274.1>

**Publisher's Note** Springer Nature remains neutral with regard to jurisdictional claims in published maps and institutional affiliations.